IEEE Access
Multidisciplinary | Rapid Review | Open Access Journal

Received January 26, 2020, accepted February 6, 2020, date of publication February 11, 2020, date of current version February 20, 2020.

Digital Object Identifier 10.1109/ACCESS.2020.2973278

Design and Modeling of Hybrid Uniplanar Electromagnetic Bandgap Power Planes for Wide-Band Noise Suppression on Printed Circuit Boards

JUNHO JOO[1], HYEON YEONG CHOI[2], AND EAKHWAN SONG[3], (Senior Member, IEEE)
[1]Department of Electrical Engineering, Missouri University of Science and Technology, Rolla, MO 65409, USA
[2]Korea Railroad Research Institute (KRRI), Gyeonggi 16105, South Korea
[3]Department of Electronics and Communications Engineering, Kwangwoon University, Seoul 01897, South Korea

Corresponding author: Eakhwan Song (esong@kw.ac.kr)

The present research was conducted by the research grant of Kwangwoon University in 2019. This work was also supported in part by the National Research Foundation of Korea (NRF) grant funded by the Korea government (MSIP) (No.NRF-2017R1C1B1008605) and in part by a grant from the R&D Program of the Korea Railroad Research Institute, Republic of Korea.

ABSTRACT In this paper, a hybrid uniplanar compact electromagnetic bandgap (UC-EBG) design is proposed with a wide-band noise suppression in power planes of printed circuit boards (PCBs). To achieve wide-band noise suppression, the proposed hybrid UC-EBG design employs a combination of various uniplanar EBG unit cells with different sizes which have different frequency ranges of noise suppression corresponding to the size of the cells. In addition, an analytic model of the EBG unit cell composed of cavity resonant model and meander line inductance is proposed and validated by 3-dimensional field simulation and measurement. To demonstrate the proposed design, a heterogeneous group of unit cells with different sizes was selected and the noise transfer function was compared with that of a conventional UC-EBG structure. The proposed hybrid UC-EBG design is experimentally verified by noise transfer function measurement with a significant expansion of the stopband up to 478 % in comparison to the conventional uniplanar EBG designs with the same area occupation.

INDEX TERMS Power noise suppression, printed circuit board, uniplanar electromagnetic bandgap.

I. INTRODUCTION

Electromagnetic bandgap (EBG) structure is designed with periodic metal patterns on dielectric substrates, which prevent the propagation of electromagnetic waves in wide and specific band of frequencies [1]–[3]. Owing to the wide bandstop properties, EBG technologies have emerged as a broadband noise isolation technique for various microwave applications. Especially for the power distribution network (PDN) designs in printed circuit boards (PCBs), EBG structures have gained ample attention as embedded planar structures for switching noise suppression as they can easily be implemented and integrated with PCBs using conventional PCB manufacturing processes [4]–[7].

The associate editor coordinating the review of this manuscript and approving it for publication was Amedeo Andreotti.

Among the various EBG structures for PCB applications, the mushroom-type EBG structures that have periodic unit cells composed of planar patches and vertical vias connected to these patches have widely been introduced [8]–[10]. To achieve a wide bandwidth of noise suppression in a compact area, several modified mushroom-type EBG structures focusing on dielectric materials and PCB stack-ups have been proposed [11], [12]. However, the vias, which are essential elements of the mushroom-type EBG structures, should be fabricated during the PCB process with limited applications during the post-fabrication stage. Uniplanar compact EBG (UC-EBG) structures, which are another type of EBG structures that employ horizontal traces instead of the vertical vias as was done in the case of mushroom-type EBGs, have been introduced [13], [14]. By replacing the loop-inductance in the mushroom-type EBG structures with the self-inductance of the traces in UC-EBG structures, the necessity of having

the vertical vias has been eliminated resulting in design and fabrication flexibility. Despite the advantages of UC-EBG structures, the compact design remains complicated due to the area occupied by the patches and horizontal traces. Although, there have been several researches on area reduction for the sophisticated UC-EBG structures [15]–[17], the researchers had primarily focused on reducing the area of the UC-EBG structure instead of bandwidth improvement efficiency.

In this paper, a hybrid UC-EBG structure composed of a variety of UC-EBG cells with different sizes and stopbands has been proposed. Based on the hybrid combination of heterogeneous unit cells in UC-EBG designs, wideband noise suppression can be achieved compared to conventional homogenous UC-EBG structures with similar area occupation. In addition, the unit cells of the proposed hybrid UC-EBG structures have been modeled using the resonant cavity model for the patches and meander line models for the horizontal traces. The proposed hybrid UC-EBG structures have been experimentally validated with 3-dimensional field simulations and measurements of noise transfer function.

II. DESIGN AND MODELING OF PROPOSED HYBRID UC-EBG STRUCTURES

The conventional UC-EBG structures consist of periodic structure of unit cells, which are homogeneous in size, shape, and composition. The size and number of unit cells determine the center frequency and suppression level of the stopband, respectively [18], [19]. To achieve wide-band noise suppression with conventional UC-EBG structures that employ a single center frequency of the stopband, numerous unit cells are required with a significant area occupation on PCBs. The proposed hybrid UC-EBG structures are composed of heterogeneous unit cells of different sizes corresponding to the multiple stopbands achieving a wide range of stopband in a limited area. In this section, a unit cell design composed of a patch and meander lines are presented. To characterize the unit cells dimensionally, an analytic model of the unit cells is proposed with the resonant cavity model and inductor models of the meander lines. Based on the proposed model, a hybrid UC-EBG structure is proposed with a combination of heterogeneous unit cells.

A. A UNIT CELL DESIGN

Figure 1 shows the unit cell design for the proposed hybrid EBG structure. The unit cell, which is square-shaped with the side length represented as W_c, is designed on a PCB with a substrate thickness of t_s. The unit cell is composed of a square patch at the center and four 1-turn meander lines at each side of the patch. The meander lines are designed using a line width and a space between the lines as W_l and S_l, respectively. The patch provides capacitance between the patch and ground plane and the meander lines display inductive behavior.

To validate the unit cell design, the reflection phase simulations with various cell sizes were conducted using ANSYS High Frequency Structural Simulator (HFSS), which is based on the finite element method (FEM). In the simulations,

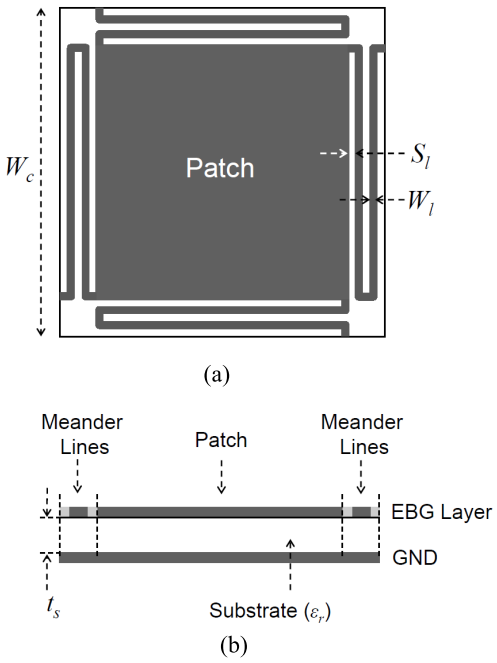

FIGURE 1. A unit cell design for the proposed hybrid EBG structure in a (a) top view (b) side view.

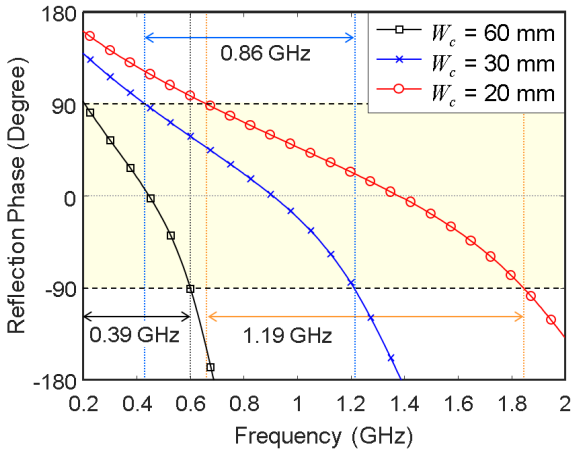

FIGURE 2. Reflection phase simulation results on the unit cell design with various cell sizes.

a FR-4 substrate with dielectric constant with substrate thickness of 4.3 and 100 um was employed and the width and space between the traces of the meander lines, W_l and S_l, are set to 100 um. Figure 2 shows the reflection phase simulation results with a cell size of 60mm, 30mm, and 20mm. The zero degree reflection phase and the frequency range for reflections phases between $\pm 90°$ for the unit cell defines the resonance operating frequency and the stopband bandwidth, respectively. In the simulation results, the unit cells exhibit their own resonance operating frequencies and the stopband bandwidths depending on the cell size as summarized in Table 1, which confirms the unit cell design can be employed as a unit element of the UC-EBG structures for the

TABLE 1. Reflection phase simulation results on the unit cell with various cell sizes.

W_c (mm)	Resonance Frequency (GHz)	Stopband Bandwidth (GHz)
60	0.44	0.39
30	0.92	0.86
20	1.38	1.19

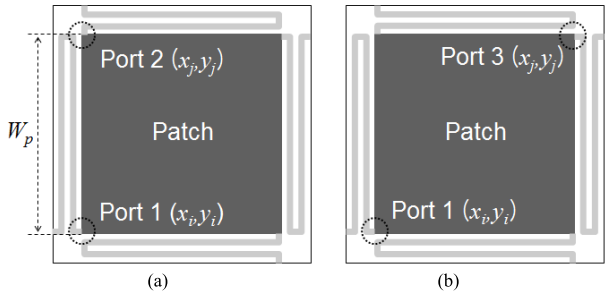

FIGURE 3. Port configurations for the self- and transfer-impedances extraction based on the resonant cavity model (a) left-top (b) left-right.

surface noise suppression. The unit cell is not restricted to a specific design but can be of any type for the UC-EBG structures that present an *LC* network. The proposed EBG structure can be implemented using a combination of the unit cells to form a distributed *LC* network with a suppression of surface-wave propagation for a specific range of frequencies.

B. UNIT CELL MODELING

In this section, an analytic model for the unit cell is proposed based on the resonant cavity model for the patch and meander line models for the horizontal traces. The patch on the PCB forms a pair of parallel plates with the ground plane and the self- and transfer-impedances can be extracted using the resonant cavity models [20]. In these models, the plane impedances can be extracted from the coordinates of the ports on the patch panel. Figure 3 shows the port configurations for the plane impedance extraction where the ports are located at the point where the patch is connected to the meander lines. Owing to the symmetry of the unit cell, a couple of two-port configurations, namely left-top and left-right, can be used to represent all the port configuration combinations. The coordinates of the ports with the left-top and left-right configuration are (0, W_p) and (W_p, W_p), respectively, where W_p is the side length of the patch shown in (1). With the coordinates, the self- and transfer-impedances of each port configuration can be obtained by using (2.1)–(2.3) where $\chi_{mn} = 1$ for $m = 0$ and $n = 0$, $\sqrt{2}$ for $m = 0$ or $n = 0$, and 2 for $m \neq 0$ and $n \neq 0$. Here, m and n are the integer values for the mode numbers, which are set to 100, a value that is large enough to ensure the accurac y of the model in a high-frequency region. k is the complex wave number to model the energy dissipation in the resonant cavity where $\tan\delta$ is the loss tangent of the dielectric substrate, and δ is the skin depth.

$$W_p = W_c - 4W_l - 6S_l \tag{1}$$

$$Z_{p\_ij}(\omega) = j\omega\mu t_s \sum_{n=0}^{\infty}\sum_{m=0}^{\infty} \frac{\chi_{mn}^2}{W_p^2\left\{\left(\frac{m\pi}{W_p}\right)^2 + \left(\frac{n\pi}{W_p}\right)^2 - k^2\right\}} \times f(x_i, y_i, x_j, y_j) \tag{2.1}$$

where

$$f\left(x_i, y_i, x_j, y_j\right) = cos\left(\frac{m\pi x_i}{W_p}\right) cos\left(\frac{n\pi y_i}{W_p}\right) cos\left(\frac{m\pi x_j}{W_p}\right) cos\left(\frac{n\pi y_j}{W_p}\right) \tag{2.2}$$

$$k = \omega\sqrt{\varepsilon_r\varepsilon_0\mu_0} - j\omega\sqrt{\varepsilon_r\varepsilon_0\mu_0}\left(\frac{\tan\delta}{2} + \frac{\delta}{2t_s}\right) \tag{2.3}$$

The meander lines of the unit cells present inductive behavior and self-inductance can be derived based on the dimensions [21]. As shown in Figure 4, the 1-turn meander line consists of five segments and the total inductance is given by the sum of self-inductances of all the segments and the mutual inductances between all the segment combinations. The self-inductance L_i of the ith segment S_i can be calculated by using (3) where the segment length l is W_p for segment 2 and 4, and S_l for segment 1, 3, and 5. The mutual inductances from the segment combinations in the 1-turn meander line are derived as shown in (4.1)–(4.3). With the extracted self- and mutual-inductances, the total inductance of the 1-turn meander line can be obtained by using (5).

$$L_i = \frac{1}{500}W_p\left[ln\left(\frac{2l}{0.2232\,(W_l + t_s)}\right) - 1.25 + \left(\frac{W_l + t_s}{3l}\right) + \frac{\mu}{4}\right] \tag{3}$$

$$M_1(W_p, S_l) = \frac{\mu_0}{2\pi}W_p\left[ln\left(\frac{W_p}{S_l} + \sqrt{1 + \left(\frac{W_p}{S_l}\right)^2}\right) - \sqrt{1 + \left(\frac{S_l}{W_p}\right)^2} + \frac{S_l}{W_p}\right] \tag{4.1}$$

$$M_2 = 0.5\left[M_1\left(2S_l, W_p\right) - 2M_1\left(S_l, W_p\right)\right] \tag{4.2}$$

$$M_3 = \frac{\mu_0}{4\pi}\left[3S_l ln\left(3S_l\right) - 4S_l ln\left(2S_l\right) + S_l ln\left(S_l\right)\right] \tag{4.3}$$

$$L_{total} = \sum_{i=1}^{5} L_i + \sum_{k=1}^{3} M_k \tag{5}$$

The two-port impedance matrix for the unit cell can be obtained by combining the patch impedance matrix and impedance of the meander lines. As shown in Figure 5, the impedance matrix for the patch [Z_p], extracted from (2), is combined with the meander line impedance Z_L, which is $j\omega L_{total}$ at each port of the matrix. Based on the definition of Z-parameters, the two-port impedance matrix of

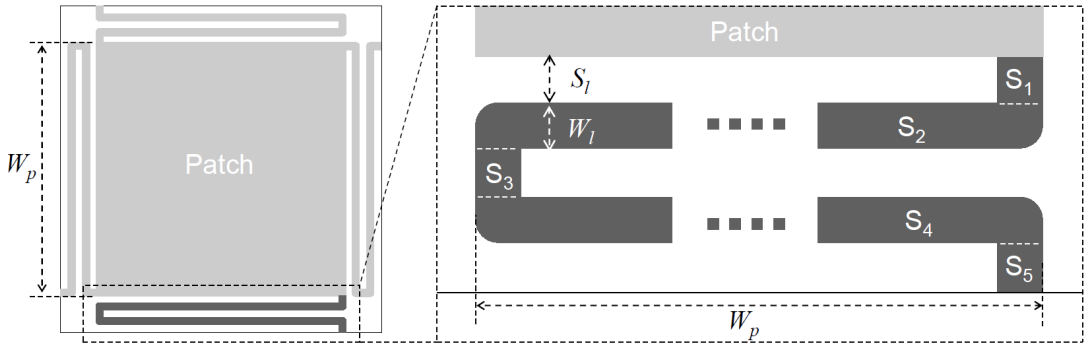

FIGURE 4. 1-turn meander line structure of the unit cell.

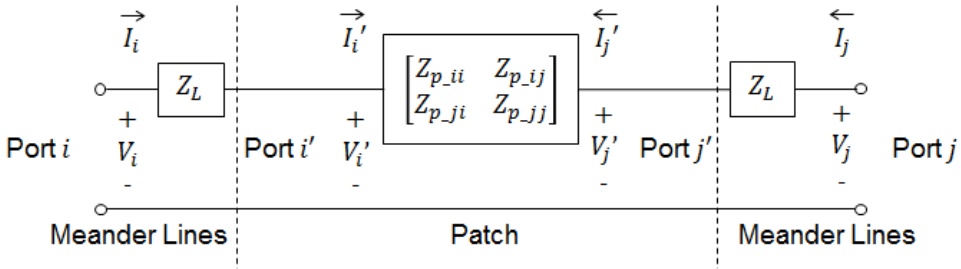

FIGURE 5. Port configurations for the self- and transfer-impedances extraction based on the resonant cavity model (a) left-top (b) left-right.

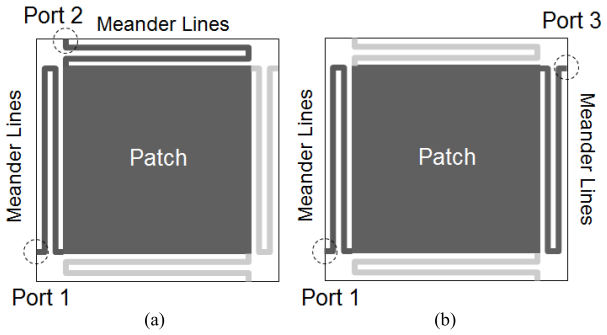

FIGURE 6. Combination of the patch and meander lines with different port configuration (a) left–top (b) left–right.

the combined structure can be synthesized by combining the impedance matrix for the patch and meander line impedance, as shown in (6).

$$Z_{ii} = Z_{jj} = \frac{V_i}{I_i}_{(I_j = I_j' = 0)} = \frac{V_i' + I_i Z_L}{I_i} = Z_L + Z_{p\_ii} \quad (6.1)$$

$$Z_{ij} = Z_{ji} = \frac{V_i}{I_j}_{(I_i = I_i' = 0)} = \frac{V_i' + I_i' Z_L}{I_j} = Z_{p\_ij} \quad (6.2)$$

The unit cell of the proposed hybrid UC-EBG has four ports at the end of the meander lines, the point from where the surface waves propagate. To complete the proposed four-port impedance matrix of the unit cell, a couple of two-port impedances of the united patch and meander lines are extracted with different port configuration. Figure 6 shows the two-port unit cell with different port configurations. The impedances of the unit cell with port configuration as left–top are equivalent to that of left–bottom and right-bottom based on the reciprocity of symmetry structure. Similarly, the impedance of a unit cell having left–right port configuration is equivalent to that of top–bottom port configuration. Based on these findings, the complete four-port impedance matrix of the unit cell can be synthesized by the two-port impedance matrices owing to the symmetry of the unit cell as shown in (7).

$$[Z] = \begin{bmatrix} Z11 & Z12 & Z13 & Z21 \\ Z21 & Z11 & Z12 & Z13 \\ Z31 & Z21 & Z11 & Z12 \\ Z12 & Z31 & Z21 & Z11 \end{bmatrix} \quad (7)$$

To validate the proposed model, the transfer function simulation and measurement were conducted, with the port assignment in Figure 6(b), using ANSYS HFSS and a vector network analyzer (VNA), respectively. Figure 7 shows the transfer functions extracted from the proposed model, 3-dimensional field simulation, and measurement with different unit cell sizes. The width and space between the traces of the meander lines, W_l and S_l, are set to 100 um, which is the minimum value that the PCB manufacturing process allows to obtain a sufficient inductance and capacitance within a limited area occupation of the unit cell. The substrate thickness, t_s, is set to 100 um, which is the typical thickness in multi-layer PCBs for consumer electronic devices. The proposed models present stopband frequencies depending on

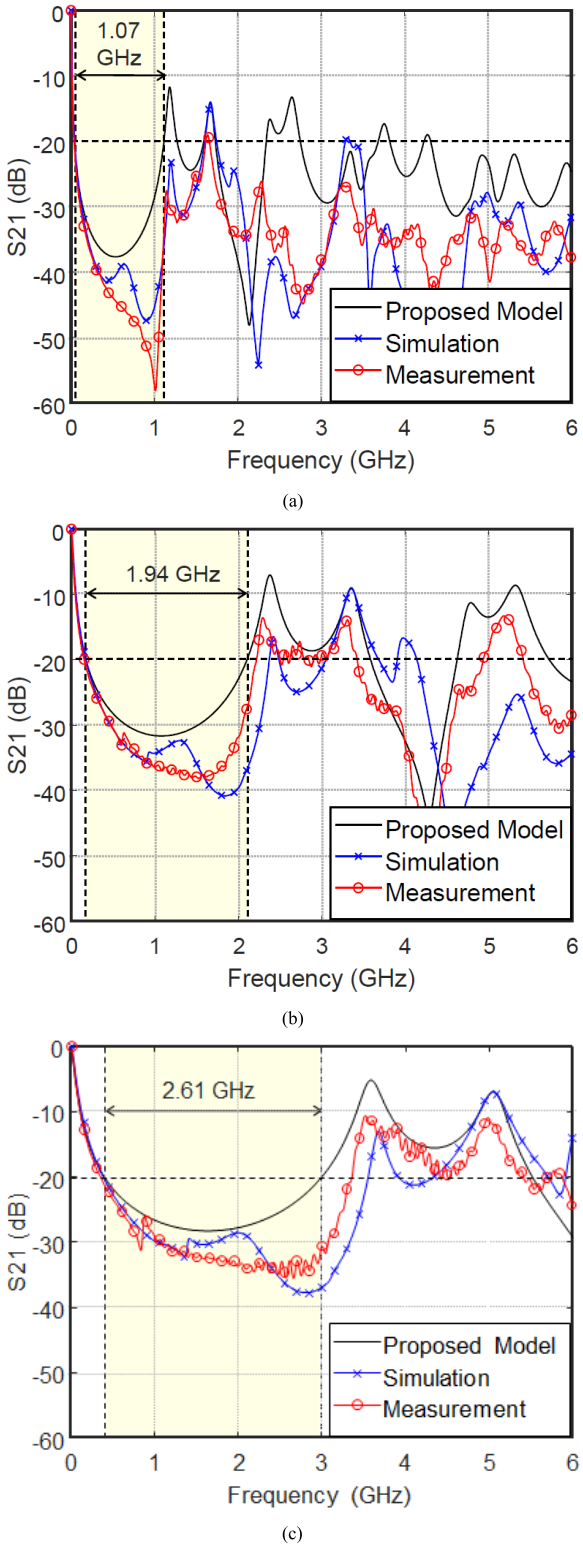

FIGURE 7. Comparison of the transfer functions of the unit cells extracted from the proposed model, 3-dimensional field simulation, and measurement with a unit cell size of (a) 60 mm, (b) 30 mm, and (c) 15 mm.

the unit cell sizes with a noticeable correlation with the simulation and measurement results. The discrepancies between the proposed models and the simulation and measurement results in high-frequency region come from using the lumped inductance models for the meander lines in the proposed models. The stopband bandwidth of the unit cells depending on the unit cell sizes with a transfer function level of −20 dB are summarized and listed in Table 2. Based on the comparison results, it can be demonstrated that the proposed analytic models can be utilized to estimate the noise suppression characteristics of the unit cells.

TABLE 2. Stopband bandwidth of the unit cells depending on the unit cell size with a transfer function level of −20 dB.

W_c (mm)	Proposed Model (GHz)	Simulation (GHz)	Measurement (GHz)
60	1.07	1.56	1.57
30	1.94	2.20	2.05
15	2.61	3.16	2.97

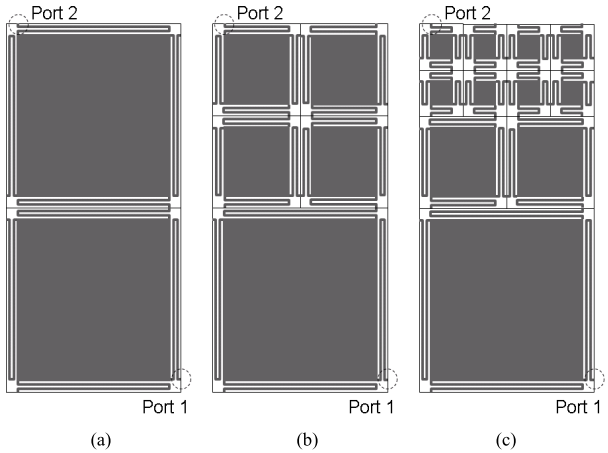

FIGURE 8. Test vehicle (TV) designs with different combination of the unit cells (a) TV 1: 60 mm × 2 (b) TV 2: 60 mm × 1, 30 mm × 4 (c) TV 3: 60 mm × 1, 30 mm × 2, 15 mm × 8.

C. PROPOSED HYBRID UC-EBG STRUCTURES

The proposed hybrid UC-EBG structures include a combination of heterogeneous unit cells of different sizes. Each unit cell exhibits a stopband corresponding to the size of the cell, and a wide range of stopbands are achieved when these differently-sized unit cells are combined with each other. Figure 8 shows the test vehicles (TVs) that are designed to validate the proposed hybrid UC-EBG structures with different combinations of the unit cells with sizes of 60 mm, 30 mm, and 15 mm. Meanwhile, the TVs are designed with a same area occupation of 7,200 mm^2. TV 1 is composed of two unit cells of size 60 mm, which is the same as that of conventional UC-EBG structures. In TV 2, one of the unit cells of TV 1 is replaced by four half-sized unit cells that are of 30 mm. In the same manner, TV 3 is designed by replacing two unit cells of 30 mm with eight half-sized unit cells of 15 mm. When the unit cells are connected, the neighboring unit cells are designed as mirror images to ensure the connectivity of the unit cells. To compare the noise

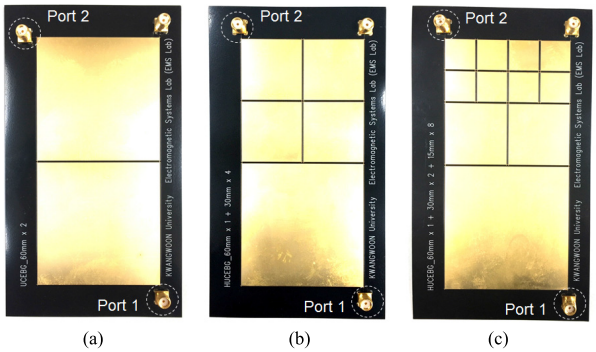

FIGURE 9. **The fabricated TVs with different combination of the unit cells: (a) TV1: 60 mm × 2 (b) TV2: 60 mm × 1, 30 mm × 4 (c) TV3: 60 mm × 1, 30 mm × 2, 15 mm × 8.**

suppression characteristics of TVs, two ports are assigned at the same locations where the surface waves come in and out.

III. EXPERIMENTAL VALIDATION

To validate the proposed hybrid UC-EBG designs, TVs were fabricated and the transfer function measurements were conducted. Figure 9 shows the TVs that were designed with the same combinations and dimensions as shown in Figure 8 on a FR-4 substrate with dielectric constant with substrate thickness of 4.3 and 100 um, respectively. As a reference board, a solid power planes without applying UC-EBG structures was also fabricated with the same dimensions with those of the TVs. The transfer functions between port 1 and port 2 of the TVs and the reference board were measured by a VNA to confirm the noise suppression performance of the proposed hybrid UC-EBG structures and they were determined to be up to 6 GHz. In addition, the analytic models of the proposed UC-EBG structures were constructed by combining the proposed unit cell models and validated, as in the previous section, and compared with the measurement results.

Figure 10 shows the comparison of the transfer functions of the proposed hybrid UC-EBG structures extracted from the proposed model and measurement. TV1 is composed of two unit cells of 60 mm in size and shows a stopband bandwidth of 0.67 GHz with a transfer function level of −60 dB below 1 GHz from the proposed model due to its homogeneous composition. TV2 and TV3 are a combination of the unit cells with different sizes to attain the benefit of the proposed hybrid UC-EBG structures. The transfer functions of TV2 and TV3 present a stopband bandwidth of 1.85 GHz and 4.21 GHz from the proposed model, respectively. Based on the mechanism of the proposed hybrid UC-EBG structures, a combination of the various unit cells presents a wider stopband owing to the combined contribution of the bandstop characteristics from each unit cell size. Therefore, TV3, which has unit cells of three sizes, exhibits a wider stopband than that of TV2, which has unit cells of two sizes, as shown in Figure 10. In addition, the proposed models for the hybrid UC-EBG are successfully demonstrated with a noticeable correlation to the transfer function measurement

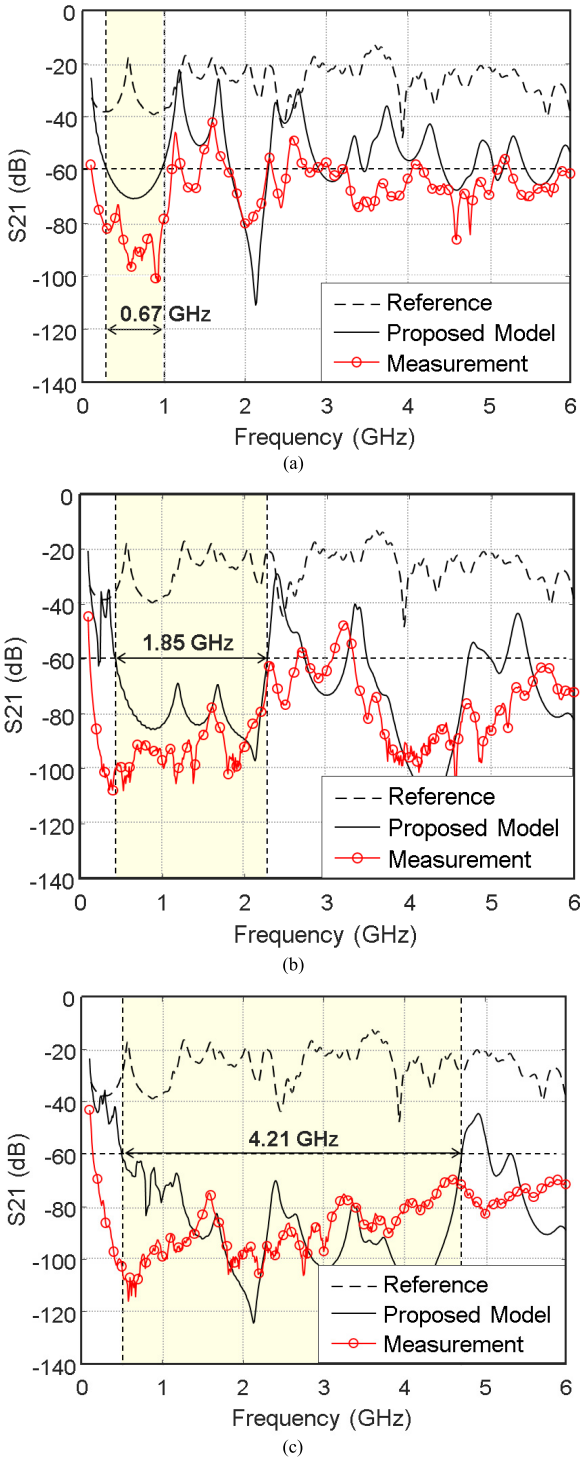

FIGURE 10. **Comparison of the transfer functions of the reference board and the proposed hybrid UC-EBG structures extracted from the proposed model and measurement (a) TV1 (b) TV2 (c) TV3.**

results. With the proposed model, the bandstop estimation of the proposed hybrid UC-EBG structures can be achieved prior to fabrication; thus, reducing the design cycle. To examine the noise suppression impact of the proposed structures, the noise suppression level is defined by the difference between the transfer functions of the TVs and the reference

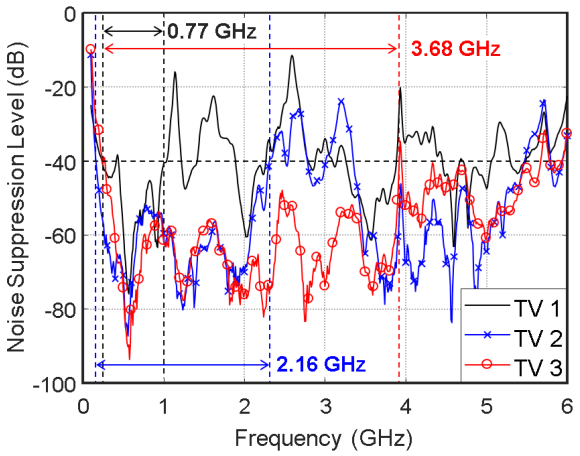

FIGURE 11. Comparison of the measured noise suppression levels of the proposed hybrid UC-EBG structures.

TABLE 3. Measured stopband bandwidth of the TVs with a noise suppression level of 40 dB.

DUT	Lower Stop Frequency (GHz)	Upper Stop Frequency (GHz)	Stopband (GHz)
TV1	0.24	1.01	0.77
TV2	0.16	2.32	2.16
TV2	0.24	3.92	3.68

board. Figure 11 shows the measured noise suppression levels of the proposed hybrid UC-EBG structures and the stopband bandwidth of the TVs associated with a noise suppression level of 40 dB as listed in Table 3. From the measurement results, it can be confirmed that the proposed hybrid UC-EBG structures can be employed to achieve a wider bandwidth of noise suppression than that of conventional designs with a limited area occupation in PCBs.

IV. CONCLUSION

In this paper, a hybrid UC-EBG design has been proposed with wide-band noise suppression in the power planes of PCBs. The proposed hybrid UC-EBG structure consists of a combination of heterogeneous unit cells of various sizes corresponding to the different frequency ranges to achieve wide-band noise suppression. To demonstrate the proposed structure, a unit cell design composed of a patch and meander lines was employed. In addition, an analytic model for the unit cells based on resonant cavity models for the patch and inductance models for the meander lines was proposed and validated using 3-dimensional field simulation and measurements. To demonstrate the proposed UC-EBG design, a heterogeneous group of unit cells with different sizes was selected and the noise transfer function was compared with that of a conventional UC-EBG structure through simulation and measurement. The proposed UC-EBG design was successfully validated by expanding the stopband by 478 % from that of a conventional design with the same area occupation. With the proposed UC-EBG design, it can be expected that wider noise suppression in a multi-functional digital device can be achieved in a small form factor. In addition, the proposed UC-EBG design can be employed with a variety of sophisticated unit cell designs to achieve further improvement in terms of bandwidth and area occupation.

REFERENCES

[1] E. Yablonovitch, "Photonic band-gap structures," *J. Opt. Soc. Amer. B, Opt. Phys.*, vol. 10, no. 2, pp. 283–295, Feb. 1993.
[2] D. Sievenpiper, L. Zhang, R. F. J. Broas, N. G. Alexopolous, and E. Yablonovitch, "High-impedance electromagnetic surfaces with a forbidden frequency band," *IEEE Trans. Microw. Theory Techn.*, vol. 47, no. 11, pp. 2059–2074, Nov. 1999.
[3] A. Sanada, C. Caloz, and T. Itoh, "Planar distributed structures with negative refractive index," *IEEE Trans. Microw. Theory Techn.*, vol. 52, no. 4, pp. 1252–1263, Apr. 2004.
[4] R. Abhari and G. V. Eleftheriades, "Metallo-dielectric electromagnetic bandgap structures for suppression and isolation of the parallel-plate noise in high-speed circuits," *IEEE Trans. Microw. Theory Techn.*, vol. 51, no. 6, pp. 1629–1639, Jun. 2003.
[5] R. F. J. Broas, D. F. Sievenpiper, and E. Yablonovitch, "A high-impedance ground plane applied to a cellphone handset geometry," *IEEE Trans. Microw. Theory Techn.*, vol. 49, no. 7, pp. 1262–1265, Jul. 2001.
[6] J. Choi, V. Govind, and M. Swaminathan, "A novel electromagnetic bandgap (EBG) structure for mixed-signal system applications," in *Proc. IEEE Radio Wireless Conf.*, Atlanta, GA, USA, Feb. 2005, pp. 243–246.
[7] E.-P. Li, X.-C. Wei, A. C. Cangellaris, E.-X. Liu, Y.-J. Zhang, M. D'amore, J. Kim, and T. Sudo, "Progress review of electromagnetic compatibility analysis technologies for packages, printed circuit boards, and novel interconnects," *IEEE Trans. Electromagn. Compat.*, vol. 52, no. 2, pp. 248–265, May 2010.
[8] S. Shahparnia and O. M. Ramahi, "Miniaturised electromagnetic bandgap structures for broadband switching noise suppression in PCBs," *Electron. Lett.*, vol. 41, no. 9, pp. 519–520, Apr. 2005.
[9] M.-S. Zhang, Y.-S. Li, C. Jia, and L.-P. Li, "A power plane with wide-band SSN suppression using a multi-via electromagnetic bandgap structure," *IEEE Microw. Wireless Compon. Lett.*, vol. 17, no. 4, pp. 307–309, Apr. 2007.
[10] C.-Y. Hsieh, C.-D. Wang, K.-Y. Lin, and T.-L. Wu, "A power bus with multiple via ground surface perturbation lattices for broadband noise isolation: Modeling and application in RF-SiP," *IEEE Trans. Adv. Packag.*, vol. 33, no. 3, pp. 582–591, Aug. 2010.
[11] J. Lee, H. Kim, and J. Kim, "High dielectric constant thin film EBG power/ground network for broad-band suppression of SSN and radiated emissions," *IEEE Microw. Wireless Compon. Lett.*, vol. 15, no. 8, pp. 505–507, Aug. 2005.
[12] J. Park, A. C. W. Lu, K. M. Chua, L. L. Wai, J. Lee, and J. Kim, "Double-stacked EBG structure for wideband suppression of simultaneous switching noise in LTCC-based SiP applications," *IEEE Microw. Wireless Compon. Lett.*, vol. 16, no. 9, pp. 481–483, Sep. 2006.
[13] F.-R. Yang, K.-P. Ma, Y. Qian, and T. Itoh, "A novel TEM waveguide using uniplanar compact photonic-bandgap (UC-PBG) structure," *IEEE Trans. Microw. Theory Techn.*, vol. 47, no. 11, pp. 2092–2098, Nov. 1999.
[14] F. Yang and Y. Rahmat-Samii, "Microstrip antennas integrated with electromagnetic band-gap (EBG) structures: A low mutual coupling design for array applications," *IEEE Trans. Antennas Propag.*, vol. 51, no. 10, pp. 2936–2946, Oct. 2003.
[15] R. Waterhouse and D. Novak, "A small electromagnetic bandgap structure," in *IEEE MTT-S Int. Microw. Symp. Dig.*, San Francisco, CA, USA, 2006, pp. 602–605.
[16] L. Kurra, M. P. Abegaonkar, A. Basu, and S. K. Koul, "A compact uniplanar EBG structure and its application in band-notched UWB filter," *Int. J. Microw. Wireless Technol.*, vol. 5, no. 4, pp. 491–498, Aug. 2013.
[17] H. Malekpoor, "Comparative investigation of reflection and band gap properties of finite periodic wideband artificial magnetic conductor surfaces for microwave circuits applications in X-band," *Int. J. RF Microw. Comput. Aided Eng.*, vol. 29, Jun. 2019, Art. no. e21874.
[18] T.-L. Wu, C.-C. Wang, Y.-H. Lin, T.-K. Wang, and G. Chang, "A novel power plane with super-wideband elimination of ground bounce noise on high speed circuits," *IEEE Microw. Wireless Compon. Lett.*, vol. 15, no. 3, pp. 174–176, Mar. 2005.

[19] J. Qin and O. M. Ramahi, "Ultra-wideband mitigation of simultaneous switching noise using novel planar electromagnetic bandgap structures," *IEEE Microw. Wireless Compon. Lett.*, vol. 16, no. 9, pp. 487–489, Sep. 2006.
[20] I. Novak and J. R. Miller, *Frequency-Domain Characterization of Power Distribution Networks*. Boston, MA, USA: Artech House, 2007, pp. 67–72.
[21] G. Stojanovic, L. Zivanov, and M. Damjanovic, "Compact form of expressions for inductance calculation of meander inductors," *Serbian J. Electr. Eng.*, vol. 1, no. 3, pp. 57–68, 2004.

JUNHO JOO received the B.S. and M.S. degrees in electronics and communications engineering from Kwangwoon University, Seoul, South Korea, in 2017 and 2019, respectively. He is currently pursuing the Ph.D. degree in electrical engineering with the Missouri University of Science and Technology (Missouri S&T), Missouri, USA. His research interests are system-level EMC/EMI, simulation-based conducted susceptibility evaluation, and development of dielectric characterization techniques for millimeter-wave applications.

HYEON YEONG CHOI received the B.S. degree in electrical engineering from the University of Seoul, Seoul, South Korea, in 2003, and the M.S. and Ph.D. degrees in electrical engineering from the Korea Advanced Institute of Science and Technology (KAIST), Daejeon, South Korea, in 2005 and 2010, respectively. From 2011 to 2013, she was a Research Engineer with KDDI Research and Development Laboratories, Inc., Japan, where she was engaged in the research and development of photonic transport networks and future optical networks. She is currently with the Korea Railroad Research Institute (KRRI), South Korea. Her research interests include integrated wireless network for railway and intelligent train control systems.

EAKHWAN SONG (Senior Member, IEEE) received the B.S., M.S., and Ph.D. degrees in electrical engineering from the Korea Advanced Institute of Science and Technology (KAIST), Daejeon, South Korea, in 2004, 2006, and 2010, respectively. In 2008, he was a Technical Co-op with the IBM Systems and Technology Group (STG), Poughkeepsie, NY, USA. In 2010, he was a Postdoctoral Researcher with KAIST, where he was engaged in high-speed signal integrity and power integrity design in system-in-package, and equalizer design in high-speed serial links. From 2011 to 2013, he was with the Global Technology Center (GTC), Samsung Electronics, as a Senior Engineer. In Samsung Electronics, he worked focusing on high-speed serial interconnects design and electromagnetic compatibility/ interference (EMC/EMI) design for ICs, packages, and highly-integrated mobile devices. He has been an Associate Professor with the Department of Electronics and Communication Engineering, Kwangwoon University, since 2014. His research interests include system-level EMC/EMI, multigigabit serial interface design, and advanced electromagnetic applications. He was a recipient of the Best Hardware Award in IBM Early Tenure TechConnect 2008.